ANALYTICAL BIOCHEMISTRY **261,** 149–158 (1998)
ARTICLE NO. AB982725

Model and Simulation of Multivalent Binding to Fixed Ligands

Kristian M. Müller, Katja M. Arndt, and Andreas Plückthun[1]
Biochemisches Institut, Universität Zürich, Winterthurerstrasse 190, CH-8057 Zürich, Switzerland

Received December 10, 1997

A model to quantitate the principal aspects of multivalent binding was developed. It describes the random distribution of an immobilized component (the ligand) taking into account local densities. The binding of a bivalent molecule (the analyte) to the ligand is described as occurring in two steps, the second of which is driven by the local concentration of neighboring ligands. The model was used to simulate the kinetics of bivalent binding in surface plasmon resonance biosensors such as BIAcore. The simulations are compared with measured data. The simulation quantitates the influence of bivalent binding on the sensor signal, as a function of ligand density, analyte concentration, and binding site distance. Such simulations will be helpful for understanding and designing experiments to assess avidity effects as well as for developing molecules with high avidity. Furthermore, they help to analyze the inherent complexity in seemingly simple sensorgrams.

Key Words: **avidity; bivalent; BIAcore; biosensor.**

Multivalent binding is an important, inherent feature of many biological systems. On the other hand, the intrinsic affinity of a single binding site is often the quantity of interest. This discrepancy has been recognized for decades in the determination of the affinity of antibodies, which are at least bivalent and thus behave different in solution and solid-phase assays.

The majority of efforts to determine true affinities have so far been directed to the reduction of bivalent binding in the experimental set-up to simplify data interpretation. For example, an antigen can often be made monomeric, and for an antibody, monovalent Fab and scFv fragments can be used. However, the aim of the work presented here is to understand the influence of bivalence on the binding. This is important for maximizing binding to cellular surfaces in therapeutic settings and for protein engineering, in order to optimize the geometry for multivalent proteins used as analytes or ligands. Thus, we primarily wish to study factors such as ligand density and binding site distance, rather than propose to extract intrinsic affinities from multivalent binding experiments. For this purpose, we have set up a microscopic kinetic model and applied it to the simulation of multivalent binding kinetics. The kinetics of multivalent binding to ligands fixed on a surface or in a three-dimensional network is of direct biological relevance, for example, when antibodies bind to epitopes on surfaces such as viruses and cells.

Bivalent and multivalent recombinant antibody fragments, named miniantibodies, have become available by protein engineering, and they mimic the natural multivalency despite being much smaller (1, 2). In this respect the question arises how the size of the bivalent molecule influences its avidity and how the avidity effect correlates with the ligand density on the surface. The quantitation of these effects is important for the comparison of different molecules and the prediction of their behavior.

Biosensors, measuring time-resolved kinetics on a surface or in a layer, allow questions of size, valency, and ligand density to be experimentally addressed. The presented simulations were performed in the context of data obtained with optical biosensors such as the BIAcore (BIACORE, Sweden) (3), the BIOS (ASI, Switzerland), and the IAsys (Fison, United Kingdom) instruments, from which the nomenclature and data visualization were derived. These instruments detect the change of refractive index in a small layer above a surface, which correlates with the absolute mass of protein present in this layer, by surface plasmon reso-

[1] To whom correspondence should be addressed. Fax: (+41-1)-635-5712. E-mail: plueckthun@biocfebs.unizh.ch.

0003-2697/98 $25.00

nance (SPR),[2] optical waveguide lightmode spectroscopy (OWLS), or resonant mirror technology, respectively. The change of protein concentration in this layer is, in the case of the BIAcore, monitored in relative resonance units (RU) versus time. Nonetheless, the simulations can be adapted to other techniques such as total internal reflection (TIR) in general and ELISA measurements.

The main concern regarding the quality of the interaction data obtained with SPR biosensors has been mass transport limitation. This problem has been extensively studied from a theoretical point of view (4–6). In general, one can conclude that for the measurement of intrinsic binding constants the ligand should be immobilized to such a low level that mass transport and multivalent binding do not interfere with a simple model. In this idealized case, only the statistical factor of two binding sites per analyte would have to be taken into account (7). However, under such conditions the multivalent binding, which is the quantity of interest in the present study, cannot be evaluated.

Attempts to calculate the influence of bivalent binding have been made before, mainly in the context of antibody binding to surfaces. In an early and often cited approach (8), the equilibrium constants of a bivalent molecule are calculated, taking into consideration the spatial relationship between the two binding sites. To be applicable, this model requires that the number of free sites within reach for the second binding step is greater than unity. Since such high immobilization densities are difficult to achieve with proteins, this requirement as well as the lack of a kinetic description unfortunately prevents its application to biosensor data, and the same restriction holds for the application of related models (9). Other bivalent binding models describe experimental data such as cell surface receptor binding (10), binding to column matrices (11), and total internal reflection microscopy (12), but again cannot be transferred to a time-resolved flow system, as they do not describe the full kinetics and the ligand density. Spatial distance of the binding sites and fixed ligands in a one-dimensional array have been used in models to calculate the exclusion effect and total valency of a polymer (13, 14). In the work presented here, the kinetics of a binding interaction is simulated in a flow system, taking into account ligand density and size of the analyte.

MATERIALS AND METHODS

The BIAcore instrument. Although the simulations described in the following section are useful for other data acquisition techniques as well, they are exemplified and visualized according to the principle and data display of the BIAcore instrument (BIAcore). The heart of the BIAcore is a small flow cell connected to an optical unit. The flow cell encloses approximately 60 nl with an active area of 1.1 mm^2 and a height of 50 μm (3). The active area is composed of an approximately 100-nm-thick dextran layer which is linked to the underside of the flow cell facing the optical unit. Protein and small molecule ligands can be coupled to the dextran layer, which has been modified to carry carboxyl groups, using standard coupling chemistry. The optical unit detects an intensity change in a totally reflected light beam due to surface plasmon resonance. Depending on the refractive index of the solution and the mass of protein, present in the dextran layer, a light beam reflected from the surface of the flow cell is modulated via its evanescent field extending into the layer. This leads to a time-dependent signal displayed in relative resonance units versus time. Although not used in general due to experimental uncertainties, the resonance units can be approximately converted to mass of protein in the dextran layer by the relation 1 RU $\approx$ 1 pg/mm^2 (15). Combining this with the approximated thickness of 100 nm for the dextran layer, the RU can be transformed to molar concentrations according to Eq. [1]:

$$\text{conc (mol/liter)} \cong \frac{\text{conc (RU)}}{100 \times M_r}. \qquad [1]$$

The simple monovalent rate equation. So far, most of the kinetic SPR biosensor data have been evaluated by a simple first-order rate equation where the analyte A, which is by definition the molecule in solution, interacts with the immobilized ligand L according to the chemical reaction

$$A + L \rightleftharpoons AL$$

The rate equation for this reaction is (c_0 denoting initial concentrations):

$$\frac{dc^{AL}}{dt} = k_{ass}\, c_0^A\, (c_0^L - c^{AL}) - k_{diss}\, c^{AL}. \qquad [2]$$

In this case, the analyte concentration of the injected solution c_0^A, which is continuously replaced, is treated as a constant. The term $c_0^L - c^{AL}$ represents the free ligand concentration. The determination of c_0^L requires the knowledge of the volume of the dextran layer as well as the amount of ligand. Both values are difficult to determine. Therefore, the standard evaluation (16) avoids the direct calculation of this concentration. However, for the simulations described here, the con-

[2] Abbreviations used: RU, resonance units; SPR, surface plasmon resonance; ELISA, enzyme-linked immunosorbent assay.

version given in Eq. [1] is accurate enough to not influence the principle and trends of the data.

The monovalent rate equation with mass transfer. As has been noted by several authors (4–6), mass transport limitation can be a problem in biosensor measurements. An important and commonly observed consequence of mass transport limitation is the rebinding phenomenon, in which dissociated analyte is not washed out but binds to another close-by ligand, leading to an artificially slowed off-rate. To compare the simulations of bivalent binding with mass-transport-limited simulations, we applied a simple model where the flow cell is divided into two compartments: first, the dextran layer where the reaction takes place, referred to with subscript R; and second, the volume above the dextran layer where the buffer is exchanged, referred to with subscript 0. The flow rate within the dextran layer can be slower than the overall flow rate according to hydrodynamic laws. Assuming laminar flow, the analyte concentration for the reaction c_R^A differs from the initial, injected concentration c_0^A by the buffer displacement in the dextran layer along the cell length, which can be neglected in the case of the BIAcore, as well as a transfer perpendicular to the dextran layer, which is dependent on the diffusion of the analyte and the geometry of the flow cell. As before, the buffer exchange above the dextran layer is treated to be infinitely fast. Thus, two chemical equations apply: $A \rightleftarrows A_{dextran}$, and $A_{dextran} + L_{dextran} \rightleftarrows AL$.

Equation [3] describes the complex formation, as does the simple rate equation (Eq. [2]), but the concentrations are now given for the dextran layer volume, where the reaction takes place. Coupled to the complex forming rate equation is a second rate equation (Eq. [4]), describing the concentration change of the analyte A, taking into account the one-dimensional flow rate ($flow_x$) in the layer compartment and cell length ($length_x$) as well as a transfer constant (k_{trans}) from the flow compartment to the layer compartment:

$$\frac{dc_R^{AL}}{dt} = k_{ass}\, c_R^A\, (c_0^L - c_R^{AL}) - k_{diss}\, c_R^{AL} \qquad [3]$$

$$\frac{dc_R^{AL}}{dt} = -k_{ass}\, c_R^A\, (c_0^L - c_R^{AL}) + k_{diss}\, c_R^{AL} + \frac{flow_x}{length_x}\,(c_0^A - c_R^A) + k_{trans}\,(c_0^A - c_R^A) \qquad [4]$$

k_{trans} can be roughly approximated independently from the flow rate, using Fick's first law and by assuming a linear concentration gradient from top to bottom of the diffusion layer of height h, with c_R being the average concentration at half height. By doing so, k_{trans} can be related to the diffusion constant D multiplied by the contact area of the layers, divided by the volume of the reaction layer, and divided by its half height, which gives $2D/h^2$. Thus, for bovine serum albumin (M_r 67 kDa) with $D = 6.1 \times 10^{-11}$ m^2 s^{-1} (17) and a layer thickness of 100 nm, the transfer rate is approximated at 1.2×10^4 s^{-1}. As the diffusion-limited layer may be thicker than the dextran matrix (4) or the flow may not be laminar, transfer rates ranging from 10^2 to 10^6 s^{-1} have been used in our simulations for a protein of 100 kDa.

The treatment of bivalent binding in solution. For bivalent binding a two-step binding mode with two bimolecular reactions is assumed, which is described by two chemical reactions. The bivalent analyte, which is injected, is named AA and the complexes formed with one or two immobilized ligands are named AAL and AALL, respectively.

$$AA + L \rightleftarrows AAL$$

$$AAL + L \rightleftarrows AALL$$

Other binding modes such as the formation and dissociation of a ternary complex may occur. For antibodies, binding proteins with an equilibrium dissociation constant typically in the range of 10^{-6} to 10^{-9} M and a ligand concentration typically between 0.05 and 1 mM, the two-step mechanism should apply to most reactions. This can be described by two reactions:

$$\frac{dc^{AAL}}{dt} = k_{ass1}\, 2\, c_0^{AA}\, (c_0^L - c^{AAL} - 2c^{AALL}) - k_{diss1}\, c^{AAL} - \frac{dc^{AALL}}{dt} \qquad [5]$$

$$\frac{dc^{AALL}}{dt} = k_{ass2}\, c^{AAL}\, (c_0^L - c^{AAL} - 2\, c^{AALL}) - 2\, k_{diss2}\, c^{AALL}\,. \qquad [6]$$

The concentration and c_0^{AA} and c^{AALL} are multiplied by a factor of two to account for the two binding sites per molecule. In other approaches this factor is frequently not present and thus implicit in either the association constant or concentration terms. To ensure that these equations, which formally describe a reaction in solution, can be fitted to experimental data with immobilized ligands, different association and dissociation rate constants are usually used for each equation (18) resulting in four parameters. However, both rate constants obtained from such fits can differ significantly from the intrinsic rate constant and no molecular in-

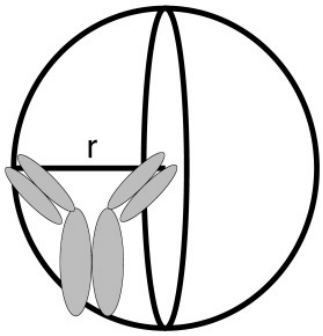

FIG. 1. Scheme of a sphere with an antibody as analyte. The access radius r is a functional term and is related to the distance between the two binding sites of the bivalent molecule (see text). The access radius might become larger than the apparent binding site distance, due to movement of the bound ligand and its support.

sight is provided, since no geometric parameters are used. Thus, we developed a new model.

The treatment of bivalent binding in a rigid matrix. The model for bivalent binding has two parts: first, a description of the ligand distribution; and second, a description of the binding reaction. The following equations refer to a layer typically present in biosensors, but can easily be transformed to describe the reaction on a surface such as an ELISA plate. An exact description of the physicochemical properties of the layer as well as its influence on molecules is difficult and is the topic of an ongoing controversial discussion (6, 18). For the model presented, it is assumed that the matrix fills uniformly a thin layer of known thickness, is rigid as a first approximation (but see below), and does not interfere with the interaction. We realize that any deviation of the real system from these assumptions will show up in any fittable parameter. Since a complete molecular description of the dextran layer is not available, we believe that these simplifying assumptions still provide insight into the main factors involved in multivalent binding. The ligand is attached to the matrix and therefore fixed in space. This assumption as well as our aim to use only one intrinsic association and dissociation rate constant for multivalent binding events requires the modification of Eq. [5] and Eq. [6].

At concentrations typically used for immobilization, the average distance of ligands is too large to allow all ligands to participate in a bivalent binding of the analyte. To account for this fact mathematically, first the whole volume V_R where the reaction takes place (the dextran layer) is quantitized into volumes V_S calculated as spheres with a radius equal to the functional distance of the two binding sites of the analyte (Fig. 1). These volumes are treated as to fill the reaction volume V_R uniformly. Second, the immobilized ligands are randomly distributed in the spheres. The proportion of spheres containing one ligand or more than one ligand, respectively, can be calculated from stochastic theory. This is an approximation of the more complex calculation of the distance distribution of ligands in space. The spheres with more than one ligand can either be treated the same or be split into spheres with two, three, and so forth ligands. For most cases, already the number with three ligands can be neglected. The number of occupied spheres can be calculated using a binomial distribution. Given the number of ligands n_0^L, the number of spheres n^s, and the number of ligands in the sphere k, the probability for this event is:

$$P(\text{sphere with } k \text{ ligands}) = \binom{n_0^L}{k}\left(\frac{1}{n^s}\right)^k\left(1-\frac{1}{n^s}\right)^{n_0^L-k}. \quad [7]$$

The binomial distribution was approximated with a Poisson distribution, since the probability is small and the number of events large and the error of this approximation is negligible.

$$P(\text{sphere with } k \text{ ligands}) = \frac{\left(n_0^L\frac{1}{n^s}\right)^k}{k!}e^{-n_0^L\frac{1}{n^s}} = \frac{(c_0^L\ V_s)^k}{k!}e^{-c_0^L V_s}. \quad [8]$$

The right-hand side of Eq. [8] is obtained, since the number of spheres n^s equals the reaction volume V_R divided by the volume of a sphere V_s ($n^s = V_R/V_S$), and the number of ligands divided by the reaction volume equals the ligand concentration. These probabilities allow us to calculate the fraction of sites which can be bound i times multivalently, or so to speak a multivalent binding factor, named multifac:

$$\text{multifac}_i = \frac{P(\text{spheres with} \geq \text{i ligands})}{P(\text{spheres with } \geq 1 \text{ ligand})}. \quad [9]$$

Using the Poisson distribution this equation can be rewritten to

$$\text{multifac}_i = \frac{1-\sum_{k=0}^{i-1}\frac{(c_0^L\ V_s)^k}{k!}e^{-c_0^L V_s}}{1-e^{-c_0^L V_s}}. \quad [10]$$

For simplicity in the following section, spheres with two or more than two ligands are treated as spheres with two ligands. Since spheres, and thus ligands, are initially separated into sites able to bind either monovalently or bivalently, two different reaction schemes can be applied with two different concentrations. Hence, the concentrations of ligands which can be

bound only monovalently c_0^{Lm} and those which can be bound bivalently c_0^{Lb} are calculated. The two reaction schemes for the monovalent only and the potential bivalent interactions are:

$$\mathrm{AA} + \mathrm{Lm} \rightleftarrows A\mathrm{Lm}$$

$$\mathrm{AA} + \mathrm{Lb} \rightleftarrows \mathrm{AALb}$$

$$\mathrm{AALb} + \mathrm{Lb} \rightleftarrows \mathrm{AALLb}$$

Here, Lm denotes a ligand which can be bound only in a monovalent state, because the next neighbors are too far away, and Lb refers to a ligand which can be bound simultaneously with a further ligand close by. The concentration of ligands which participate only in monomeric binding can be calculated using the probability derived above:

$$c_0^{\mathrm{L}} = \frac{n^{\mathrm{s}}}{V_{\mathrm{R}}} P(\text{sphere with one ligand}) = \frac{1}{V_{\mathrm{S}}} P(\text{sphere with one ligand}) \; . \quad [11]$$

The concentration of ligands which can undergo bivalent binding is the difference from the total ligand concentration:

$$c_0^{\mathrm{Lb}} = c_0^{\mathrm{L}} - c_0^{\mathrm{Lm}} \; . \quad [12]$$

For the purely monovalent reaction, where the analyte can reach only one ligand, the rate equation is

$$\frac{dc^{\mathrm{AALm}}}{dt} = k_{\mathrm{ass}}\, 2\, c^{\mathrm{AA}}(c_0^{\mathrm{Lm}} - c^{\mathrm{AALm}}) - k_{\mathrm{diss}}\, c^{\mathrm{AALm}} \; . \quad [13]$$

For the bivalent reaction scheme, the rate equation for the second step becomes more complicated, compared to the reaction in solution. The model needs to take into account that for the second step toward the bivalent binding, the overall concentration of the analyte in the solution becomes irrelevant and a local concentration applies, with one analyte binding site and one or more additional free ligands per sphere volume. For the bivalent case with two ligands in a sphere, one of which is unoccupied and ready for the second binding event, the relevant molecular concentration for this second closure is $1/V_{\mathrm{s}}$ for the analyte and $1/V_{\mathrm{s}}$ for the ligand. To correct the units to mol/liter, a division by Avogadro's number is further required. However, this rate expression applies only when one ligand is occupied and one ligand is free. Thus, two probability factors need to be introduced: $c^{\mathrm{AALb}}/c_0^{\mathrm{Lb}}$ for one ligand occupied and $c^{\mathrm{Lbfree}}/c_0^{\mathrm{Lb}}$ for one place free. Taken together, the coupled rate equations are

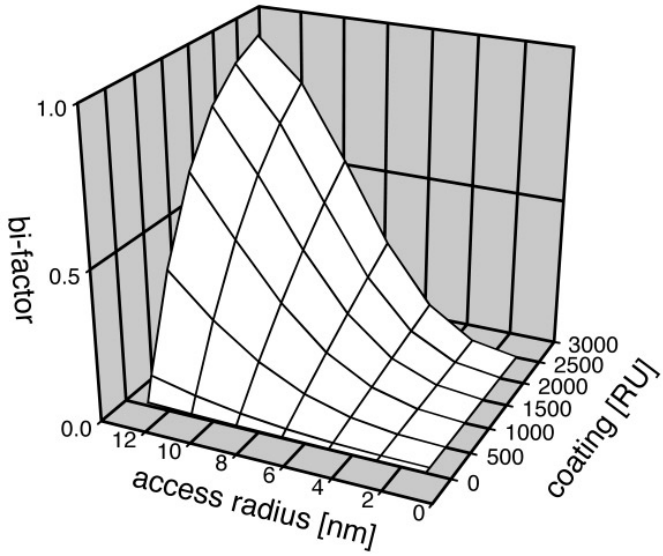

FIG. 2. Dependence of the multivalent factor ($\mathrm{multifac}_{i=2}$) for a bivalent analyte molecule on binding site distance r and immobilized ligand concentration. The multivalent factor gives the fraction of immobilized ligands, which are able to be part of a bivalent complex. The ligand density is given in relative resonance units for a 30-kDa protein by using the formula conc [mol/liter] ≈ conc [RU] × 0.01 × M_{r}^{-1}.

$$\frac{d^{\mathrm{AALb}}}{dt} = k_{\mathrm{ass}}\, 2\, c^{\mathrm{AA}}(c_0^{\mathrm{Lb}} - c^{\mathrm{AALb}} - 2\, c^{\mathrm{AALLb}}) - k_{\mathrm{diss}}\, c^{\mathrm{AALb}} - \frac{dc^{\mathrm{AALLb}}}{dt} \quad [14]$$

$$\frac{dc^{\mathrm{AALLb}}}{dt} = k_{\mathrm{ass}} \frac{1}{V_{\mathrm{s}} N_{\mathrm{A}}} \frac{c^{\mathrm{AALb}}}{c_0^{\mathrm{Lb}}} \frac{1}{V_{\mathrm{s}} N_{\mathrm{A}}} \times \frac{c_0^{\mathrm{Lb}} - c^{\mathrm{AALb}} - 2\, c^{\mathrm{AALLb}}}{c_0^{\mathrm{Lb}}} - 2\, k_{\mathrm{diss}}\, c^{\mathrm{AALLb}} \; . \quad [15]$$

The bivalent case can easily be extended to higher orders of binding. For an i times valent binding, i differential equations are required. The local concentration after the second binding step is then calculated by $(i - 1)/V_{\mathrm{s}}$.

RESULTS

The multivalent factor. A new description for the distribution of ligands was developed. By subdividing the reaction space into spheres, an easy to use stochastic formula for the distribution of ligands was obtained. A multivalent factor was derived (Eq. [10]), which gives the probability that an analyte binds to a ligand which

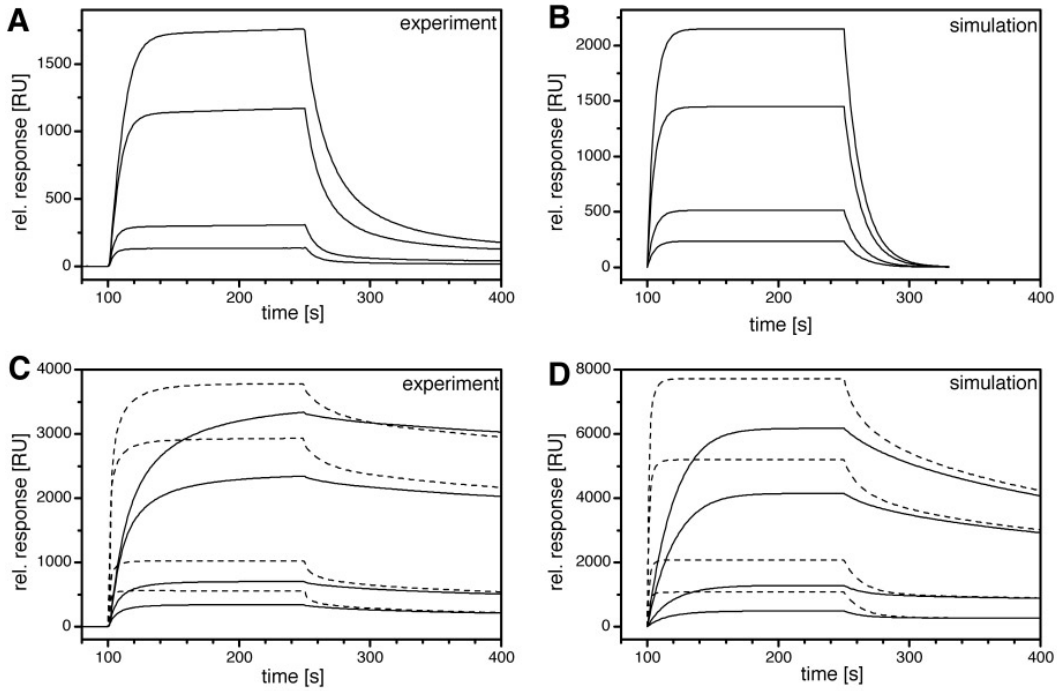

FIG. 3. Measurement and simulation of monovalent and bivalent binding of His-tagged proteins to an immobilized anti-His-tag antibody as seen on a BIAcore instrument. The antibody was coated to give 1100, 2400, 6767, and 10,000 RU. The rate constants used for simulation were previously determined from a system with 1:1 interaction. (A) Measurement of a monomeric 27-kDa His-tagged protein. (B) Simulation of the experiment seen in A, using a first-order rate equation (Eq. [2]). (C) Measurement of a dimeric His-tagged protein of 101 kDa at two concentrations of (—) 50 nM and (- - -) 1 μM. (D) Simulation of the experiment seen in C using the presented model (Eqs. [14] and [15]) with an access radius of 11 nm (see text). The monomeric protein probably contains a small fraction of dimers, explaining why the curves in A do not return to baseline and the crossover seen in C at the highest immobilization density is caused by an incomplete regeneration.

is located such that a second binding is possible. This multimeric factor is dependent on the ligand density, as well as on the access radius, which describes the volume swept out by the second binding site once the first has bound to an immobilized ligand. Figure 2 illustrates the contribution of radius and ligand density to the multivalent factor for a bivalent molecule. For convenience the ligand density is given here in resonance units of the BIAcore instrument for a 30-kDa protein, which are easily transformed to mol/liter units by Eq. [1]. Given an estimation about the access radius, this plot allows one to judge to what extent measurements are influenced by bivalent binding.

Correlation of model and experiments. To investigate whether the model correlates with experimental measurements, an anti-His-tag murine monoclonal IgG2b antibody, named 3D5 (19), and a monomeric as well as a dimeric C-terminal His-tagged protein (20) were chosen as a model system. The protein with one His-tag was a single-chain Fv fragment with a molecular weight (M_r) of 27 kDa. The protein with two His-tags was the homodimeric yeast citrate synthase with a M_r of 50 kDa for the monomer. The molecular weight of the antibody was approximated with 150 kDa, and its two binding sites were treated independently. The anti-His-tag antibody was coupled at increasing concentrations to a BIAcore sensor chip surface. The final coating densities obtained were 1100, 2400, 6767, and 10,000 RU. The association and dissociation rate constants of His-tag binding by the antibody were determined with the monomeric protein in a series of measurements at concentrations ranging from 100 to 1600 nM at the lowest coating density of 1100 RU and a flow rate of 30 μl/min to minimize mass transfer limitations. These measurements resulted in a k_{ass} of $2.2 \times 10^5\ M^{-1}\ s^{-1}$ and a k_{diss} of $0.075\ s^{-1}$ obtained by a global fit (20). For comparison with simulations, three measurements were performed on all four surfaces. First, the monomeric protein was measured at a concentration of 500 nM (Fig. 3A). This measurement provides information about mass transport limitation and rebinding. Second, the dimeric His-tagged protein was measured at two concentrations of about 50 nM and 1 μM. Thus, in the graph two concentrations as well as four coating densities are shown (Fig. 3C).

Simulations of the differential equations for monovalent (Eq. [2]) and bivalent binding (Eqs. [13], [14], and [15]) were performed with the program ISIM (21) employing a fifth-order Sarafyan–Runge–Kutta algorithm with a maximum time step of 0.01 s. As the

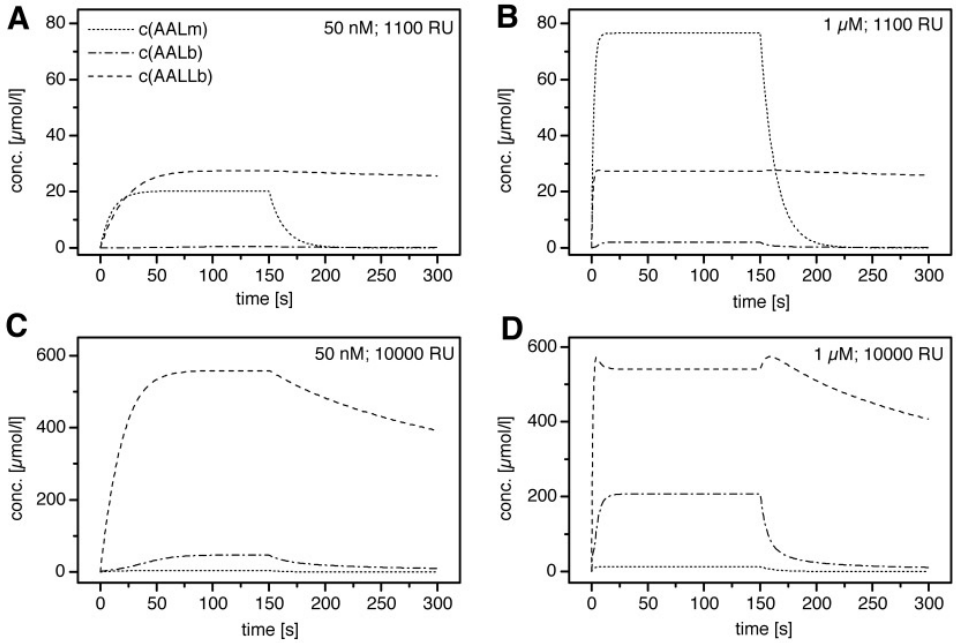

FIG. 4. Time course of (···) monovalently bound species in a monovalent sphere (one ligand in a sphere), of (- · -) monovalent bound species in a bivalent sphere (two ligands in a sphere), and of (- - -) bivalent bound species at two concentrations and two coating densities as seen in the simulation for the dimeric protein in Fig. 3D. (A) 50 nM protein concentration, 1100 RU coating density. (B) 1 μM, 1100 RU. (C) 50 nM, 10,000 RU. (D) 1 μM, 10,000 RU.

calculations are based on concentrations, but the signal of the BIAcore is given in resonance units, the coating density was transformed to molar concentrations and the final signal back to RU according to Eq. [1]. Concentrations in the simulation were constrained to positive values.

For the simulation of the monovalent binding (Fig. 3B) all parameters were predetermined by experimental values. For the simulation of the bivalent binding the access radius had to be varied. According to the X-ray structure of the homologous porcine citrate synthase (PDB: 4 cts) (22) the distance between the C-termini is 3.1 nm. However, a radius of this size results in mainly monomeric binding in the simulation and does not correlate with the experimental data. Since the His-tagged protein (the analyte) is bound by an immobilized antibody (the ligand), the access radius is likely influenced by the size and flexibility of the antibody. Therefore, a radius of 11 nm was chosen, as it reproduced best the shape of all curves (Fig. 3D). The access sphere calculated from molecular dimensions is extended by the molecular displacement of the ligand which only requires that the rotational correlation time and any diffusion of the complex with its dextran matrix is shorter than the average lifetime of the complex. Thus, the interpretation of the access radius should not be taken as a static geometric measure, since any flexibility in the dextran network and ligand linkage may increase the access radius, regardless of the binding site distance in the bivalent analyte. Despite not directly reproducing geometric properties such as molecule size and orientation, the model reproduces well the key elements of the experimental data over a wide range of coating densities as well as analyte concentrations. As seen in both the monovalent and bivalent case, the absolute signal is not satisfactorily reproduced. This might be explained by the exponentially decaying detection sensitivity with distance from the surface as well as nonlinearities in the mass detection, both making the conversion of resonance units to concentrations not straightforward.

Dissection of binding. According to the model described above, three molecular species contribute to the measured signal in the case of bivalent binding: monovalently bound analyte in a "monovalent" sphere (AALm), monovalently bound analyte in a "bivalent" sphere (AALb), and bivalently bound analyte in a "bivalent" sphere (AALLb). In a monovalent sphere only one ligand is present, whereas in a bivalent sphere the analyte can reach another ligand. In the simulation, the concentration of these can be looked at separately. A dissection of the simulation (Fig. 3D) is given in Fig. 4. The time course of the three components is plotted for two concentrations (50 nM and 1 μM) as well as for two coating densities (1100 and 10,000 RU). At the low coating density of the ligand the major fraction of the binding sites is mono-

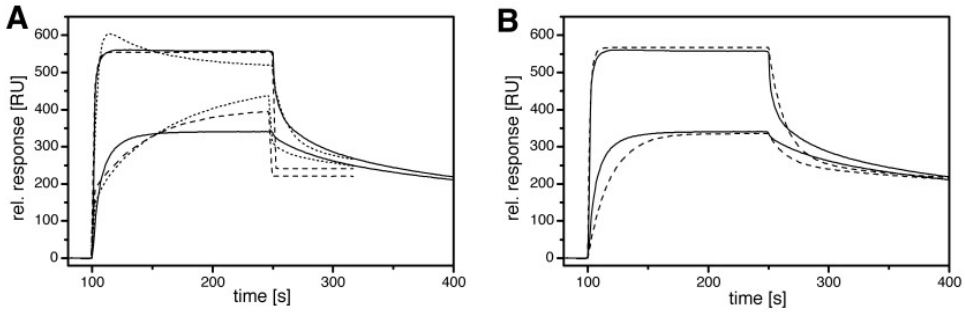

FIG. 5. Comparison of fits to experimental data using a standard model (Eqs. [5] and [6]) for bivalent binding (A) and the presented model (Eqs. [14] and [15]) with fixed ligands (B). The solid line in both panels represents the measured data on a 1100 RU surface obtained at 50 nM (lower curve) and 1 μM (upper curve) analyte concentration. (A) Global least-square curve fit using a solution model with individual free maximum signal and free individual bulk effect (baseline): (- - -) all rate constants set to predetermined values obtained from the monovalent experiment; (· · ·) only the first equation set to the predetermined rate constants. (B) Manual fit of measured data using the fixed ligand model with predetermined rate constant values for both rate equations. A 14-nm access radius was chosen and an additional global scaling factor of 0.58 was used for both curves.

valent. As expected, the equilibrium concentration of the monovalent binding (c^{AALm}) is higher than the bivalent binding (c^{AALLb}) at the low ligand density (Figs. 4A and 4B), while the reverse is true for the higher ligand concentration (Figs. 4C and 4D). When compared at constant ligand density (Fig. 4A compared to 4B, and Fig. 4C compared to 4D), the equilibrium of the bivalently bound concentration (c^{AALLb}) is reached faster in the case of the higher analyte concentration, but both high and low analyte concentrations end up at the same level of resonance units, since all bivalent sites are saturated. In the case of the high coating density nearly all sites can be bound bivalently. Since in this case a significant part of spheres carries more than two ligands, our simulation, which takes into account only one ligand for the second binding step, becomes a crude approximation. It is possible that additional steric requirements may prevent access to multiple ligands. In the case of the low analyte concentration (Fig. 4C), the bivalently bound component clearly dominates. At the high analyte concentration some monovalently bound component (c^{AALb}) can be seen as well as an unexpected dip in the bivalently bound species (Fig. 4D). This is caused by the competition of binding of two monovalently bound molecules with the binding of one bivalently bound molecule, due to the high analyte concentration. Apart from the latter case, monovalently bound molecules in a bivalent sphere are hardly detected.

Comparison of the new model with a currently used model. For the empirical evaluation of bivalent binding two differential equations might be used in the form of Eq. [5] and Eq. [6], which treat the two-step binding process as if completely free in solution, but with different rate constants for each step. Thus, up to four parameters are required, if no constraints are used. Unfortunately, this conventional model is not very informative about the processes underlying the observed curves. Such a model, in which constraints according to the known relations between the rates were applied, was compared with the fixed ligand model presented here. We tested how well the measured data at 50 nM and 1 μM analyte concentrations injected on the 1100 RU surface were reproduced. For the conventional approach the measured data were simulated using Eq. [5] and Eq. [6] or fitted with standard fitting software (BIAevaluation 3.0), in which the calculation for the second step was performed in resonance units. In the latter case a global fit was used with a free maximum signal for each curve, which corresponds to using the ligand density as a free parameter, and free individual bulk effects, which allows for a baseline shift. However, two alternative sets of constraints were imposed. Either the association and dissociation rate constants for both steps in the solution model (Eq. [5] and Eq. [6]) were set to the values previously measured with a monomeric analyte or only the first step (Eq. [5]) was set to these values, while the rate constants for the second step (Eq. [6]) were fitted. As expected and demonstrated in Fig. 5A, it was impossible to fit the data. With all rate constants constrained, the total off-rate is close to zero, as all molecules bind bivalently and switch only between the first and second differential equation. With only the first step constrained, nonphysical rate constant values had to be selected for the second step. With completely free choice of rate constants, a satisfactory fit was obtained (data not shown). The rate constants determined in the latter case, however, deviated significantly from the data determined with a monomeric ligand. Introducing mass transfer limitation into a monovalent binding according to Eq. [3] and Eq. [4] did not result in a satisfactory fit either (data not shown). This demonstrates that there are cases where the free, four-pa-

rameter fit (with two independent on- and off-rates) is very difficult to interpret in meaningful terms.

For the fixed ligand model, all rate constants as well as the ligand density are determined by the values known from experiments of a monomeric ligand, and a satisfactory reproduction of the experimental curve was obtained even though no baseline shift was allowed (Fig. 5B). The signal intensity was directly calculated from the concentrations and the molecular weight. However, in addition to the access radius, which in the ideal case would be the only variable, the dextran layer thickness had to be reduced to 58 nm for conversion of molar concentrations to RUs to account for the absolute size of the signals. Since the program used for simulations did not allow fitting, approximations of the measured data were obtained by manual variation of the parameters. As seen in Fig. 5B, the principal course of the kinetics, especially with regard to the biphasic dissociation phase, was reproduced. The access radius was set to 14 nm, which must be seen as a composite value accounting for the movement of the analyte bound to a large molecule linked at one position and the clustering of binding sites to pairs, since an antibody is immobilized.

DISCUSSION

A theoretical description of ligand distribution, a method to calculate a two-step binding process, and a comparison of simulated data with measurements of the BIAcore instrument are presented. It was shown that the model reproduces key elements of bivalent binding, such as ligand-dependent contribution of monovalent and bivalent binding. The purpose of this study was not to extract true intrinsic binding constants from such measurements, but to contribute to an understanding of the major factors determining multivalent binding. The intention of the model was to highlight the influence of fixing ligands in space at various densities on bivalent binding. Current approaches, however, do not regard such geometric factors and either are based on interaction in solution (as implemented in the BIAevaluation software) or lack a distinct ligand distribution (9).

Molecular details could not be taken into account in our model for two reasons. First, detailed steric knowledge is not available for most experiments; and second, too many parameters would be obtained, making it difficult to pinpoint the important properties. Of course, assuming a molecular size for all involved molecules, restraining binding to one side of the molecule, reducing the sphere size, and allowing binding to neighboring spheres would bring the model closer to reality. With enough computer power at hand, a random seed of realistic ligands in space and simulation of binding of real analytes including laws for hydrodynamics and molecular motion might become possible. However, the dispute about whether the dextran layer influences binding or not (6, 18), and how flexible it is, demonstrates that, before detailed models can be applied, more experimental facts need to be uncovered. Mass transport limitation according to Eq. [4] has been tested in the simulations, but turned out not to be of relevance, at least for the low immobilization densities where the reaction calculated without mass transport limitation is slower than the measured reaction. At the high immobilization densities (10,000 RU) the reaction calculated without mass transport is indeed faster then the measured reaction indicating that mass transport limitation plays a role. However, such high concentrations are a borderline case for the use of the model presented here due to steric complications, as not all ligand sites can be filled simultaneously. We are aware of the fact that in exact physical terms already the immobilization of a molecule to a dextran layer is an approximation to kinetics in solution, since the degrees of freedom are reduced. Thus, the access radius is to be taken as a factor encompassing all these uncertainties.

The model presented here does explain well the biphasic behavior of binding kinetics and its dependence on the surface density. To compare simulations with measurements, an anti-His-tag antibody and a dimeric His-tagged protein were chosen. The radii of the access sphere found necessary to reproduce experimental data were large compared to the size of the analyte. Radii of 11 to 14 nm were used, whereas a geometric consideration gives an approximate radius of 9 nm comprising 3 nm between the two His-tags and 6 nm for the flexible Fab fragment to which it is bound. The longer effective radius has most likely two reasons. First, the immobilization of an antibody does not result in a statistical distribution of binding sites, and a larger access radius can account for the clustering of binding sites. Thus, the calculation of the dimer factor as presented is critical for this case, but the use of the presented rate equations is not affected. We used this experimental set up as it is suited to visualize the effect of bivalent binding. Second, the assumption of a fully rigid matrix may not hold in practice for the dextran layer as it is used in the BIAcore cell. The latter explanation is supported by the observation that receptors immobilized in the dextran layer as monomers can be dimerized by analytes such as peptidic hormones (23), suggesting mobility of the dextran fibers. The second rate equation in the multivalent model presented is likely to overestimate association, as steric hindrance is not taken into account. Therefore, the calculated rates in the bivalent case are likely to be faster than in reality.

A problem in relating the model to the experiments performed with the BIAcore is the correlation of resonance units to protein concentrations. This is difficult to calculate, as the response plateau reached during

association seen on various surfaces with increasing coating densities does not correlate with calculations [at the highest coating density, a lower signal of bound analyte than expected from an extrapolation of the lowest coating density is seen (Fig. 1C)]. Since this behavior can be seen in measurements with other proteins as well (data not shown), this might witness a nonlinearity in the detection method, depending on the analyte size and total signal, and/or a steric hindrance of the bound analyte, making it impossible to bind every ligand simultaneously. Taking this together with the assumption of all ligands being functional, the ligand concentration has likely been overestimated.

An alternative explanation for the presented measurements would be a continuos, sequential binding of one or the other binding site to ligands in the matrix, which would constitute an increased rebinding for bivalent molecules. As a wobbling between two ligands is automatically included in the model, the only difference to the model presented here would be that in a model which relies only on rebinding, no bivalent binding occurs at all. It is difficult to make this distinction in an experiment directly. However, BIAcore measurements with monovalent molecules at high coating density, and therefore high probability for rebinding, maintain their characteristic curve shape for association and dissociation and do not show a similarity to the curve shape of bivalent molecules at a low immobilization density. Thus, we believe that the current model is helpful for the understanding of multivalent action and thus for assaying and designing multivalent molecules.

ACKNOWLEDGMENTS

We thank Joannis Apostolakis for helpful discussion and Dr. Benno Arbenz for introduction to the ISIM program.

REFERENCES

1. Pack, P., and Plückthun, A. (1992) *Biochemistry* **31,** 1579–1584.
2. Pack, P., Müller, K., Zahn, R., and Plückthun, A. (1995) *J. Mol. Biol.* **246,** 28–34.
3. Jönsson, U., Fägerstam, L., Ivarsson, B., Johnsson, B., Karlsson, R., Lundh, K., Löfas, S., Persson, B., Roos, H., Rönnberg, I., Sjölander, S., Stenberg, E., Stahlberg, R., Urbaniczky, C., Östlin, H., and Malmqvist, M. (1991) *Biotechniques* **11,** 620–627.
4. Glaser, R. W. (1993) *Anal. Biochem.* **213,** 152–161.
5. Schuck, P., and Minton, A. P. (1996) *Anal. Biochem.* **240,** 262–272.
6. Schuck, P. (1996) *Biophys. J.* **70,** 1230–1249.
7. Kalinin, N. L., Ward, L. D., and Winzor, D. J. (1995) *Anal. Biochem.* **228,** 238–244.
8. Crothers, D. M., and Metzger, H. (1972) *Immunochemistry* **9,** 341–357.
9. Kaufman, E. N., and Jain, R. K. (1992) *Cancer Res.* **52,** 4157–4167.
10. DeLisi, C., and Chabay, R. (1979) *Cell Biophys.* **1,** 117–131.
11. Hogg, P. J., Reilly, P. E., and Winzor, D. J. (1987) *Biochemistry* **26,** 1867–1873.
12. Pisarchick, M. L., and Thompson, N. L. (1990) *Biophys. J.* **58,** 1235–1249.
13. Pincus, M. R., DeLisi, C., and Rendell, M. (1981) *Biochim. Biophys. Acta* **675,** 392–396.
14. Macken, C. A., and Perelson, A. S. (1986) *IMA J. Math. Appl. Med. Biol.* **3,** 71–97.
15. Stenberg, E., Persson, B., Roos, H., and Urbaniczky, C. (1991) *J. Colloid Interface Sci.* **143,** 513–526.
16. Karlsson, R., Michaelsson, A., and Mattsson, L. (1991) *J. Immunol. Methods* **145,** 229–240.
17. Cantor, C. (1980) Techniques for the Study of Biological Structure and Function, Freeman, New York.
18. Karlsson, R., and Fält, A. (1997) *J. Immunol. Methods* **200,** 121–133.
19. Lindner, P., Bauer, K., Krebber, A., Nieba, L., Kremmer, E., Krebber, C., Honegger, A., Klinger, B., Mocikat, R., and Plückthun, A. (1997) *Biotechniques* **22,** 140–149.
20. Müller, K. M., Arndt, K. A., and Plückthun, A. (1998) *Anal. Biochem.* **259,** 54–61.
21. Dunn, I. J., Heinzle, E., Prenosil, J. E., and Ingham, J. (1992) Biological Reaction Engineering, VCH-Verlagsgesellschaft, Weinheim, Germany.
22. Wiegand, G., Remington, S., Deisenhofer, J., and Huber, R. (1984) *J. Mol. Biol.* **174,** 205–219.
23. Cunningham, B. C., and Wells, J. A. (1993) *J. Mol. Biol.* **234,** 554–563.